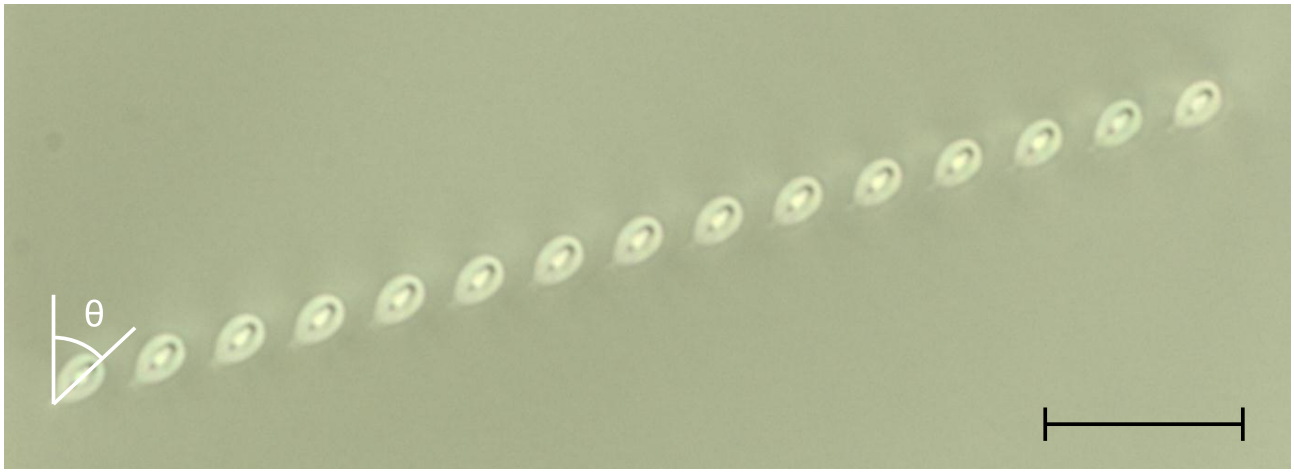

Supplementary Figure 1: Waveguide reproducibility at different depths. Microscope images of the cross sections of the array of tilted waveguides fabricated at different depths. The deepest is buried 230 μm below the substrate top surface. The vertical spacing between the waveguides is 5 μm while the orizontal one is 20 μm. The tilt angle of the waveguides is $\theta = 41°$. The scale-bar corresponds to 50 μm.

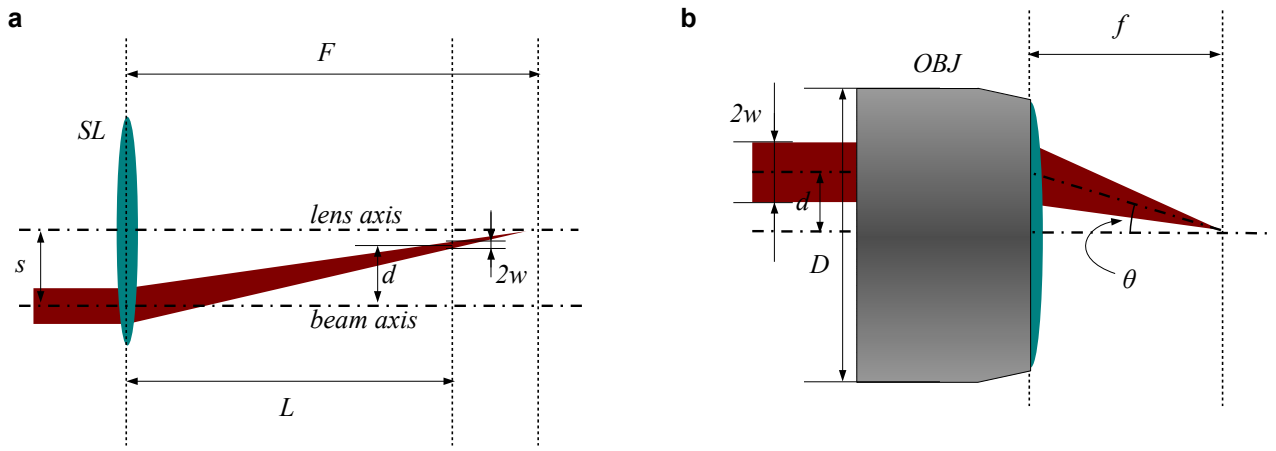

Supplementary Figure 2: Geometric schemes of the writing beam transformation through the optical elements. (a) Geometric scheme representing the beam displacement d induced by a spheric lens SL of focal length F, at a distance L, for a transverse offset s of the lens itself. (b) Geometric scheme representing the writing laser beam tilted by an angle θ when impinging on the objective (OBJ) in an off-center position, with a displacement d; f is the focal length of the objective and $2w$ is the beam waist diameter.

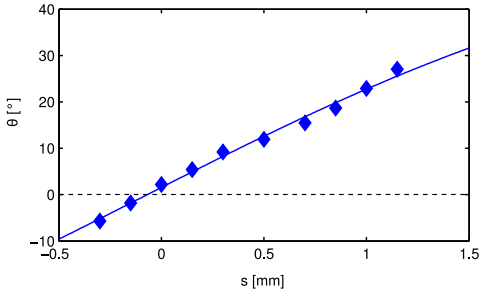

Supplementary Figure 3: Calibration of waveguide tilt. Experimental calibration of the achieved waveguide-axis tilt θ for a translation s of the spheric lens. Diamonds represent experimental points, while the solid line represents a best-fit with a curve of the form expressed in Eq. (2) of Supplementary Note 1 with parameters: $C = 0.39$ mm^{-1} and $s_0 = -0.069$ mm.

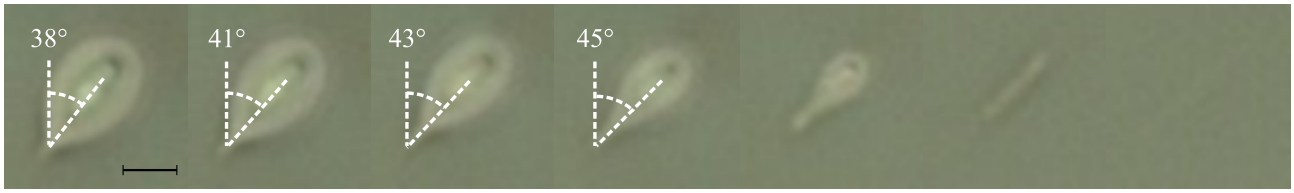

Supplementary Figure 4: Waveguide tilt achieves 45°. Microscope images of the cross sections of the waveguides fabricated with $2w = 0.75$ mm. The black scale-bar is 5 μm long.

Input State	Fidelity A	Fidelity B
H	0.995 ± 0.003	0.980 ± 0.003
V	0.962 ± 0.003	0.984 ± 0.003
D	0.964 ± 0.006	0.966 ± 0.005
A	0.956 ± 0.006	0.982 ± 0.004
R	0.987 ± 0.003	0.990 ± 0.003
L	0.969 ± 0.004	0.970 ± 0.004

Supplementary Table 1: Single-qubit fidelities. Fidelities of single qubit quantum state tomography measurements, corresponding to different polarization states: horizontal (H), vertical (V), diagonal (D), antidiagonal (A), right- (R) and left- (L) circular- for both input modes A (central column) and B (right column).

SUPPLEMENTARY NOTE 1

Details of the waveguide fabrication setup

Positioning of the spheric lens

As discussed in the Main Text, a spheric lens SL with focal length $F = 50$ cm is mounted on a linear translation stage in our waveguide writing setup. This lens is used to obtain both a spot-size reduction of the writing laser beam and an effective transverse displacement of the laser beam itself on the aperture of the high-NA objective.

The effective numerical aperture NA_{eff} at which the objective operates depends on the ratio between the beam diameter $2w$ and the objective entrance diameter D. In particular, one can consider that the full numerical aperture ($NA = 1.4$) is achieved if $2w = D$ while for lower values of $2w$ a linear relation holds as a first approximation: $NA_{\text{eff}} \sim NA\frac{2w}{D}$. We experimentally characterized the beam spot-size as a function of the distance L from the lens SL and we found that $2w$ =1.6 mm for $L = 44$ cm, which gives $NA_{\text{eff}} \sim 0.5$ since $D = 4.5$ mm (see Supplementary Fig. 2 for illustration of the relevant geometrical parameters).

Experimental characterization of the waveguide cross section rotation

The angle defining the propagation direction of the beam after the objective, which determines the tilt angle of the optical axis of the fabricated waveguide, can be worked out easily by looking at Supplementary Fig. 2b:

$$\theta = \arctan\left(\frac{d}{f}\right) = \arctan\left(s\frac{L}{fF}\right) \tag{1}$$

Note that this formula is calculated under the approximation of a collimated beam that impinges orthogonally on the objective aperture, thus neglecting the small angular deviation θ_D of the beam caused by the translation of the lens. This approximation is reasonable since $F \gg f$ and thus the resulting focal distance after the objective is practically not affected by the presence of the lens. The second order effects caused by θ_D will be discussed in Sec. 3 of this Supplementary Note.

In the experimental practice, to accurately calibrate our fabrication process, we fabricated waveguides with different lens displacement s and measured the resulting θ (see Supplementary Fig. 3). The measured points were fitted with a curve of the form:

$$\theta = \arctan\left[(s - s_0)\, C\right] \tag{2}$$

where C and s_0 are free parameters. C comprises the different geometrical parameters of the setup, while s_0 allows to compensate for non-perfect centering of the spheric lens. This characterization shows that the experimental configuration described in the previous paragraph permits us to fabricate waveguides with the cross section tilted up to $\theta_{max} = 27°$ (see Fig. 2 of the Main Text). This value is limited by the maximum beam displacement d achievable for a given beam spot size $2w$, without having it cut by the objective aperture edge.

As a matter of fact, we tried to extend the angular range obtainable with our technique in order to reach the value of $\theta = 45°$, which would allow to perform arbitrary operations on light polarization in a simpler and more compact fashion. The strategy we adopted was to further reduce the beam spot diameter down to $2w = 0.75$ mm by placing the spheric lens at $L = 54$ cm. Note that this value is greater than the nominal focal distance of the lens ($F = 50$ cm); nevertheless the beam is still converging at the objective entrance, due to the slight divergence of our femtosecond laser beam. In Supplementary Fig. 4 it can be observed that with this new configuration it is possible to get much higher values of θ, but the goal value of $\theta = 45°$ is very close to the region where the waveguide is degraded. In fact, to achieve this angle the beam must be displaced towards the edge of the objective aperture. For this reason we decided to fabricate the integrated device presented in the Main Text using the first configuration, with $2w = 1.6$ mm and waveguide tilts up to $\theta = 27°$. It is understood that, as shown in Supplementary Note 2, this choice does not preclude any polarization state preparation.

Effects of the lens translation on the objective focal position

The displacement d of the beam on the objective aperture, as a function of the transverse displacement s of the lens with respect to the axis of the incoming beam, can be calculated as

$$d = \frac{L}{F}s \tag{3}$$

as it is evident from the geometric construction in Supplementary Fig. 1a.

The angular deflection of the beam impinging on the objective is

$$\theta_D \simeq \frac{d}{L} = \frac{s}{F} \tag{4}$$

note that in our experiments typically $|s| < 2$ mm thus $\theta_D < 0.2°$. As mentioned in the Main Text, this small deflection θ_D may cause a small transverse displacement of the focal spot after the writing objective, with respect to the ideal case where the beam impinging on the objective is always parallel to the objective axis. This results in a lateral offset between waveguide segments written with different shifts s (i.e. with different rotations of the optical axis). However, these offsets are highly reproducible and therefore can be effectively compensated by translating the sample of the opposite amount when writing the different segments. In particular, when writing the integrated QST circuit that we present in the main text, an 11.2 μm lateral offset had to be compensated between the waveguide sections at 0° and 22.5°.

Waveguides at different depths

Lastly, to show that our technique allows to fully exploit the three-dimensional capabilities of femtosecond laser micromachining, we fabricated an array of tilted waveguides, each of them buried in the substrate at a different depth, ranging from 160 μm to 230 μm below the sample surface. During the array fabrication we kept a constant lens displacement $d = 2$ mm. In Supplementary Fig. 1 one can appreciate that the shape and the dimension of the waveguide cross-section, as well as its tilt angle, remain substantially unaltered when changing the fabrication depth. This is made possible by the use of an immersion oil objective, which avoids the aberrations and refractive effects at the air-glass interface.

SUPPLEMENTARY NOTE 2

Description of the polarization state and waveplate operation

We will recall in this Note some basic formalism describing the polarization state of a photon and the action of a birefringent waveplate, and we will show that by combining the integrated waveplates presented in the Main Text it is possible to implement arbitrary waveplate operations.

The polarization state of a single photon may be described by the state vector:

$$|\Psi\rangle = \alpha|H\rangle + \beta|V\rangle \tag{5}$$

where $|H\rangle$ and $|V\rangle$ are two orthogonal polarization eigenstates, corresponding to a linear polarization state parallel to the x axis and y axis respectively. The vector $J = \begin{bmatrix}\alpha \\ \beta\end{bmatrix}$ corresponds to the Jones vector describing the classical polarization state of a coherent beam.

The evolution of the polarization state of a photon propagating through a linear optical element, according to the formalism of the Jones vectors and matrices, is given by a linear matrix operation on the vector J:

$$J' = MJ \tag{6}$$

where M is a 2×2 matrix describing the optical element. For a generic waveplate (or birefringent medium), having the fast axis at an angle θ with respect to the x axis and inducing a phase delay δ between the two polarization components, it holds:

$$M(\theta, \delta) = \begin{bmatrix} \cos^2\theta + e^{i\delta}\sin^2\theta & \left(1 - e^{i\delta}\right)\sin\theta\cos\theta \\ \left(1 - e^{i\delta}\right)\sin\theta\cos\theta & e^{i\delta}\cos^2\theta + \sin^2\theta \end{bmatrix} \tag{7}$$

Observing the form of the matrix (7) one can easily notice that waveplates with different values of θ and δ may be equivalent, in particular:

$$M(\theta, \delta) = M(\theta + \pi, \delta) \tag{8}$$

$$M(\theta, \delta) = e^{-i\delta} \cdot M\left(\theta - \frac{\pi}{2}, -\delta\right) \tag{9}$$

where the common phase factor $e^{-i\delta}$ in the second equivalence has no influence on the polarization state. This means that a set of waveplates with $\theta \in \left[-\frac{\pi}{4};\frac{\pi}{4}\right)$ and $\delta \in [0;2\pi)$ is sufficient to perform every waveplate operation.

One can further show that an even smaller set of waveplates is sufficient, provided that one decomposes the action of a single generic waveplate into the action of several cascaded waveplates of this smaller set. As an example (the decomposition is not unique), one can combine a half-waveplate at an angle θ:

$$M(\theta,\pi) = \begin{bmatrix} \cos 2\theta & \sin 2\theta \\ \sin 2\theta & -\cos 2\theta \end{bmatrix} \tag{10}$$

a waveplate with phase delay δ and $\theta = 0$:

$$M(0,\delta) = \begin{bmatrix} 1 & 0 \\ 0 & e^{i\delta} \end{bmatrix} \tag{11}$$

and again a half-waveplate $M(\theta,\pi)$ at the same angle θ of the first one. As can be easily calculated, the combination of these three waveplates gives:

$$M(\theta,\pi)\cdot M(0,\delta)\cdot M(\theta,\pi) = M(2\theta,\delta) \tag{12}$$

This implies that by combining three waveplates with $\theta \in \left[-\frac{\pi}{8};\frac{\pi}{8}\right)$ and $\delta \in [0;2\pi)$ as in (12), and considering the equivalences (8),(9), it is possible to reproduce the operation of an arbitrary waveplate belonging to the full set $\theta, \delta \in [0;2\pi)$.

It is thus proved that, notwithstanding the limitations in the range of angles achievable by the integrated waveplates reported in the Main Text, it is still possible to reproduce arbitrary waveplate operations.

SUPPLEMENTARY NOTE 3

Single-photon quantum state tomography measurements

In this Note we report on single-qubit quantum-state-tomography measurements realized by means of the integrated-optics device, fabricated by femtosecond laser micromachining. By starting from pairs generated by spontaneous parametric down conversion in a nonlinear crystal (see Fig. 4b of the Main Text), we generate single photon states: one photon of the pair is used as trigger for coincidence counts, while the other one is encoded in the polarization degree of freedom by means of a polarizing beam splitter, a half- and a quarter-waveplate. By this strategy, we prepare single photons in six different states of polarization: horizontal (H), vertical (V), diagonal (D), antidiagonal (A), right- (R) and left- (L) circular and deliver them to the device, which projects each incoming state into the six polarizations H, V, D, A, R, L, as widely described in the Main Text. These projections allowed us to reconstruct the density matrix of the incoming light through quantum state tomography [1]. These measurements have been performed for photons injected in both modes A and B (see Fig. 4a in Main Text). In Supplementary Table 1 we report the obtained fidelities, i.e. the overlap, between the expected density matrices and the experimental ones. The average fidelity has been found to be $\bar{\mathcal{F}} = 0.976 \pm 0.003$. Errors are computed from Poissonian statistics of coincidence counts.

SUPPLEMENTARY REFERENCE

[1] James, D.F.V, Kwiat, P.G., Munro, W.J. & White, A.G. Measurement of qubits. *Phys. Rev. A* **64**:052312 (2001).